J|A|C|S
ARTICLES
Published on Web 03/15/2007

The Structures and Electronic Configuration of Compound I Intermediates of *Helicobacter pylori* and *Penicillium vitale* Catalases Determined by X-ray Crystallography and QM/MM Density Functional Theory Calculations

Mercedes Alfonso-Prieto,[†] Anton Borovik,[‡] Xavier Carpena,[§] Garib Murshudov,[||] William Melik-Adamyan,[‡] Ignacio Fita,[§] Carme Rovira,*[,†,#] and Peter C. Loewen*[,⊥]

Contribution from the Centre especial de Recerca en Química Teòrica, Parc Científic de Barcelona, Josep Samitier 1-5, 08028 Barcelona, Spain, Institute of Crystallography of Russian Academy of Sciences, Lenisky Prospekt 59, 119333 Moscow, Russia, Institut de Biologia Molecular de Barcelona-CSIC and Institut de Recerca Biomèdica, Parc Científic de Barcelona, Josep Samitier 1-5, 08028 Barcelona, Spain, Structural Biology Laboratory, Department of Chemistry, University of York, Heslington, York YO10 5YW, England, and Department of Microbiology, University of Manitoba, Winnipeg, Canada MB R3T 2N2

Received June 5, 2006; E-mail: ploewen@ms.umanitoba.ca; crovira@pcb.ub.es

Abstract: The structures of *Helicobacter pylori* (HPC) and *Penicillium vitale* (PVC) catalases, each with two subunits in the crystal asymmetric unit, oxidized with peroxoacetic acid are reported at 1.8 and 1.7 Å resolution, respectively. Despite the similar oxidation conditions employed, the iron−oxygen coordination length is 1.72 Å for PVC, close to what is expected for a Fe=O double bond, and 1.80 and 1.85 Å for HPC, suggestive of a Fe−O single bond. The structure and electronic configuration of the oxoferryl heme and immediate protein environment is investigated further by QM/MM density functional theory calculations. Four different active site electronic configurations are considered, $Por^{\bullet+}-Fe^{IV}=O$, $Por^{\bullet+}-Fe^{IV}=O\cdots HisH^{+}$, $Por^{\bullet+}-Fe^{IV}-OH^{+}$ and $Por-Fe^{IV}-OH$ (a protein radical is assumed in the latter configuration). The electronic structure of the primary oxidized species, $Por^{\bullet+}-Fe^{IV}=O$, differs qualitatively between HPC and PVC with an A_{2u}-like porphyrin radical delocalized on the porphyrin in HPC and a mixed A_{1u}-like "fluctuating" radical partially delocalized over the essential distal histidine, the porphyrin, and, to a lesser extent, the proximal tyrosine residue. This difference is rationalized in terms of HPC containing heme b and PVC containing heme d. It is concluded that compound I of PVC contains an oxoferryl $Por^{\bullet+}-Fe^{IV}=O$ species with partial protonation of the distal histidine and compound I of HPC contains a hydroxoferryl $Por-Fe^{IV}-OH$ with the second oxidation equivalent delocalized as a protein radical. The findings support the idea that there is a relation between radical migration to the protein and protonation of the oxoferryl bond in catalase.

Introduction

Heme containing catalases are present in almost all aerobically respiring organisms.[1] They play critical roles in protecting the cell against the toxic effects of hydrogen peroxide (H_2O_2) by degrading it to water and oxygen:

$$2H_2O_2 \rightarrow 2H_2O + O_2 \qquad (1)$$

The ubiquity of the enzyme and the easy availability of substrates (H_2O_2 and alkylhydroperoxides) have made catalases the focus of many biochemical and molecular biology studies over the years.[2] It is generally accepted that the "catalatic reaction" occurs in two steps. In the first step (reaction 2), the Fe^{III}-heme reacts with H_2O_2 cleaving it such that one of the peroxide oxygen atoms becomes water and the second becomes coordinated to the iron to form compound I (Cpd I). Two electrons are removed from the heme in this process, one from the iron atom, which becomes Fe^{IV}, and the second from the porphyrin, which acquires cation radical character producing a spin state for Cpd I of $S = {}^3/_2$ (three unpaired electrons).[1,3,4]

[†] Centre especial de Recerca en Química Teòrica.
[‡] Institute of Crystallography of Russian Academy of Sciences.
[§] Institut de Biologia Molecular de Barcelona-CSIC and Institut de Recerca Biomèdica.
[||] University of York.
[⊥] University of Manitoba.
[#] Institució Catalana de Recerca i Estudis Avançats (ICREA), Passeig Lluís Companys 23, 08018 Barcelona, Spain.

(1) Nichols, P.; Fita, I.; Loewen, P. C. Enzymology and structure of catalases. In *Advanced Inorganic Chemistry;* Sykes, A. G., Mauk, G., Eds.; Academic Press: New York, 2001; Vol. 51, pp 51−106.
(2) Chelikani, P.; Fita, I.; Loewen, P. C. *Cell. Mol. Life Sci.* **2004**, *61*, 192−208.
(3) Benecky, M. J.; Frew, J. E.; Scowen, N.; Jones, P.; Hoffman, B. M. *Biochemistry* **1993**, *32*, 11929−11933.
(4) (a) Deiseroth, A.; Dounce, A. L. *Physiol. Rev.* **1970**, *50*, 319−375. (b) Dunford, H. B. *Heme Peroxidases;* Wiley: New York, 1999. (c) Veitch, G.; Smith, A. T. Horseradish peroxidase. In *Advanced Inorganic Chemistry;* Sykes, A. G., Mauk, G., Eds.; Academic Press: New York, 2001; Vol. 51, pp 107−162.

$$\text{Enz (Por}-\text{Fe}^{\text{III}}) + H_2O_2 \rightarrow \text{Cpd I (Por}^{\bullet+}-\text{Fe}^{\text{IV}}=\text{O}) + H_2O \quad (2)$$

In the second step (reaction 3), Cpd I reacts with another molecule of H_2O_2 and the enzyme returns to the resting state[5] with the axial oxygen atom becoming water and both oxygen atoms of the O_2 molecule originating from the peroxide.

$$\text{Cpd I (Por}^{\bullet+}-\text{Fe}^{\text{IV}}=\text{O}) + H_2O_2 \rightarrow \text{Enz (Por}-\text{Fe}^{\text{III}}) + H_2O + O_2 \quad (3)$$

At low H_2O_2 concentrations and in the presence of some organic electron donors, compound I may undergo a one-electron reduction to form compound II (Cpd II). In this process, the porphyrin accepts one electron, thus losing its radical character, and the spin state becomes $S = 1$ (i.e., two unpaired spins).[1,6] Cpd II of bovine liver catalase (BLC) can subsequently be converted to an inactive form of the enzyme, compound III, in a reaction with another molecule of hydrogen peroxide.[7] The protonation state of Cpd II in heme-containing proteins (peroxidases, catalases, and myoglobin) has recently received considerable attention,[8−15] and the consensus is that Cpd II of several heme-containing proteins bears a hydroxoferryl moiety instead of the traditional oxoferryl group:

$$\text{Cpd I (Por}^{\bullet+}-\text{Fe}^{\text{IV}}=\text{O}) + \text{AH} \rightarrow \text{Cpd II (Por}-\text{Fe}^{\text{IV}}-\text{OH}) + \text{A(ox)}^{\bullet} \quad (4)$$

Cpd I, the only intermediate of the catalatic reaction (reactions 2 and 3), was first detected by Chance in 1947 upon reaction of native BLC with peroxoacetic acid.[16] A decrease of the Soret band and the shift in the charge-transfer band between 600 and 700 nm in the UV absorbance spectrum along with a characteristic green color constitutes the signature of Cpd I.[1] ENDOR experiments of *Micrococcus lysodeikticus* catalase Cpd I (MLC-I) showed that its electronic structure can be described in terms of a $S = {}^3/_2$ oxoferryl (Fe═O) moiety in a ferromagnetic interaction with a porphyrin π-cation radical,[3] similar to the situation in *Proteus mirabilis* catalase (PMC).[17] It has also been shown that, when reacting the enzyme with peroxoacetic acid at 0 °C, BLC forms first the typical porphyrin-based radical followed by one electron transfer from a residue in the protein, giving rise to the oxoferryl−tyrosyl radical intermediate.[18] The latter species has been often denoted compound II*[19,20] (Cpd II*) because its spectral features are similar to Cpd II. However, use of the Cpd II* notation introduces an element of structural ambiguity because it implies the loss of only one electron from the native protein (i.e., only one oxidation equivalent above the resting state of the enzyme), whereas overall the protein-heme complex has lost two electrons, as in the classic Cpd I. Hereafter we will use the notation of Cpd I*.[21] Migration of the porphyrin radical into the protein has also been detected in other heme-containing proteins such as cytochrome c peroxidase (CcP),[22b] the catalase-peroxidases (KatG),[23,24] myoglobin (Mb)[25] and cytochrome P450.[26]

Even though it is generally assumed that Cpd I contains an oxoferryl (Fe═O) moiety, recent crystallographic structures suggest that Cpd I of CcP,[22a] MLC,[28] and BpKatG[23] have longer than expected Fe−O bond lengths (~1.9 Å) (Table 1) consistent with a hydroxoferryl group similar to that characterized in Cpd II of myoglobin.[27] In all these cases, a protein radical appears to be formed, suggesting that there could be a correlation between protonation of the oxoferryl unit (thus lengthening of the Fe−O bond) and formation of Cpd I*. This is also consistent with Cpd I* being isoelectronic with Cpd II in the hydroxoferryl heme. In other words, electron transfer to the porphyrin, regardless of whether the electron is exogenous or endogenous, facilitates protonation of the oxoferryl group.

Determination of the structures of reaction intermediates of peroxidases and, presumably, catalases can be complicated by their photoreduction during X-ray irradiation[8,29] creating a mixture of reaction intermediates of different oxidation states. Because the Fe−O(H) single bond length of Cpd II (determined experimentally at 1.80−1.92 Å[8,27,28,30] and calculated at 1.77−1.81 Å[9,10,13−15a]) is longer than a pure Fe═O bond (determined experimentally at 1.70−1.76 Å[8,33] and calculated at 1.63−1.70 Å,[10,11,13,31,32]), a mixture of photoreduction-generated Cpd II with

(5) Schonbaum, G. R.; Chance, B. Catalase. In *The Enzymes*; Boyer, P. D., Ed.; Academic Press: New York, 1976; Vol. 13, pp 363−408.
(6) (a) Deiseroth, A.; Dounce, A. L. *Physiol. Rev.* **1970**, *50*, 319−375. (b) Dunford, H. B. *Heme Peroxidases;* Wiley: New York, 1999. (c) Veitch, G.; Smith, A. T. Horseradish peroxidase. In *Advanced Inorganic Chemistry;* Sykes, A. G., Mauk, G., Eds.; Academic Press: New York, 2001; Vol. 51, pp 107−162.
(7) Lardinois, O. M. *Free Radical Res.* **1995**, *21*, 251−274.
(8) Berglund, G. I.; Carlsson, G. H.; Smith, A. T.; Szoke, H.; Henriksen, A.; Hajdu, J. *Nature* **2002**, *417*, 463−468.
(9) Nilsson, K.; Hersleth, H. P.; Rod, T. H.; Andersson, K. K.; Ryde, U. *Biophys. J.* **2004**, *87*, 3437−3447.
(10) Rovira, C. *Chem. Phys. Chem.* **2005**, *6*, 1−8.
(11) Silaghi-Dumitriescu, R. *J. Biol. Inorg. Chem.* **2004**, *9*, 471−476.
(12) Green, M. T.; Dawson, J. H.; Gray, H. B. *Science* **2004**, *304*, 1653−1656.
(13) Hersleth, H. P.; Ryde, U.; Rydberg, P.; Gorbitz, C. H.; Andersson, K. K. *J. Inorg. Biochem.* **2006**, *100*, 460−476.
(14) Carpena, X.; Wiseman, B.; Deemagarn, T.; Singh, R.; Switala, J.; Ivancich, A.; Fita, I.; Loewen, P. *EMBO Rep.* **2005**, *6*, 1156−1162.
(15) (a) Green, M. T. *J. Am. Chem. Soc.* **2006**, *128*, 1902−1906. (b) Behan, R. K.; Green, M. T. *J. Inorg. Biochem.* **2006**, *100*, 448−459.
(16) Chance, B. *Acta Chem. Scand.* **1947**, *1*, 236−267.
(17) Ivancich, A.; Jouve, H. M.; Sartor, B.; Gaillard, J. *Biochemistry* **1997**, *36*, 9356−9364.
(18) Ivancich, A.; Jouve, H. M.; Gaillard, J. *J. Am. Chem. Soc.* **1996**, *118*, 12852−12853.
(19) Hillar, A.; Nicholls, P.; Switala, L.; Lowen, P. C. *Biochem. J.* **1994**, *300*, 531−539.
(20) Zámocky, M.; Koller, F. *Prog. Biophys. Mol. Biol.* **1999**, *72*, 19−66.
(21) Hiner, A. N. P.; Raven, E. L.; Thorenley, R. N. F.; Carcia-Canovas, F.; Rodriguez-Lopez, J. N. *J. Inorg. Biochem.* **2002**, *91*, 27−34.
(22) (a) Bonagura, C. A.; Bhaskar, B.; Shimizu, H.; Li, H.; Sundaramoorthy, M.; McRee, D. E.; Goodin, D. B.; Poulos, T. L. *Biochemistry* **2003**, *42*, 5600−5608. (b) Sivaraja, M.; Goodin, D. B.; Smith, M.; Hoffman, B. M. *Science* **1989**, *245*, 738−740.
(23) Ivancich, A.; Jakopitsch, C.; Auer, M.; Un, S.; Obinger, C. *J. Am. Chem. Soc.* **2003**, *125*, 14093−14102.
(24) Jakopitsch, C.; Obinger, C.; Un, S.; Ivancich, A. *J. Inorg. Biochem.* **2006** *100*, 1091−1099.
(25) Lardinois, O. M.; Ortiz de Montellano, P. M. *Biochemistry* **2004**, *43*, 4601−4610.
(26) Schuenemann, V.; Lendzian, F.; Jung, C.; Contzen, J.; Barra, A.-L.; Sligar, S. G.; Trautwein, A. X. *J. Biol. Chem.* **2004**, *279*, 10919−10930.
(27) Hersleth, H. P.; Dalhus, B.; Görbitz, C. H.; Andersson, K. K. *J. Biol. Inorg. Chem.* **2002**, *7*, 299−304.
(28) Murshudov, G. N.; Grebenko, J. A.; Branningan, J. A.; Antson, A. A.; Barynin, V. V.; Dodson, G. G.; Dauter, Z.; Wilson, K.; Melik-Adamyan, W. R. *Acta Crystallogr., Sect. D: Biol. Crystallogr.* **2002**, *58*, 1972−1982.
(29) Gouet, P.; Jouve, H. M.; Williams, P. A.; Andersson, I.; Andreoletti, P.; Nussaume, L.; Hajdu, J. *Nat. Struct. Biol.* **1996**, *3*, 951−956.
(30) Maté, M.; Murshudov, G.; Bravo, J.; Melik-Adamyan, W.; Loewen, P. C.; Fita, I. Heme-catalases. In *Handbook of Metalloproteins;* Messerschmidt, A., Huber, R., Poulos, T., Wieghardt, K., Eds.; John Wiley & Sons: Chichester, U.K., 2001.
(31) (a) Deeth, R. J. *J. Am. Chem. Soc.* **1999**, *121*, 6074−6075. (b) Green, M. T. *J. Am. Chem. Soc.* **2001**, *123*, 9218−9219. (c) Bathelt, C. M.; Mulholland, A. J.; Harvey, J. N. *Dalton Trans.* **2005**, 3470−3476.
(32) (a) Derat, E.; Cohen, S.; Shaik, S.; Altun, A.; Thiel, W. *J. Am. Chem. Soc.* **2005**, *127*, 13611−13621. (b) Derat, E.; Shaik, S. *J. Phys. Chem. B* **2006**, *110*, 10526−10533. (c) Derat, E.; Shaik, S. *J. Am. Chem. Soc.* **2006**, *128*, 8185−8198.
(33) (a) Jouve, H. M.; Andreoletti, P.; Gouet, P.; Hajdu, J.; Gagnon, J. *Biochemie* **1997**, *79*, 667−671. (b) Andreoletti, P.; Pernoud. A.; Sainz G.; Gouet, P.; Jouve, H. M. *Acta Crystallogr., Sect. D: Biol. Crystallogr.* **2003**, *59*, 2163−2168.

Table 1. Catalase and Peroxidase Cpd I or Cpd I* Crystal Structures

protein [PDB accession no.]	heme	resolution	Fe–O length	ref
M. lysodeikticus catalase [1GWF]	heme b	2.0	1.87	28
P. vitale catalase [2IUF]	heme d	1.7	1.72 /1.72[a]	this work
H. pylori catalase [2IQF]	heme b	1.8	1.80/1.85[a]	this work
P. mirabilis catalase [1MQF]	heme b	2.5	1.76	33
horseradish peroxidase [1HCH]	heme b	1.6	1.70	8
cytochrome c peroxidase [1ZBZ]	heme b	1.3	1.87	22a
B. pseudomallei KatG [2B2R]	heme b	1.9	1.88	23

[a] Values corresponding to the two independent protein subunits.

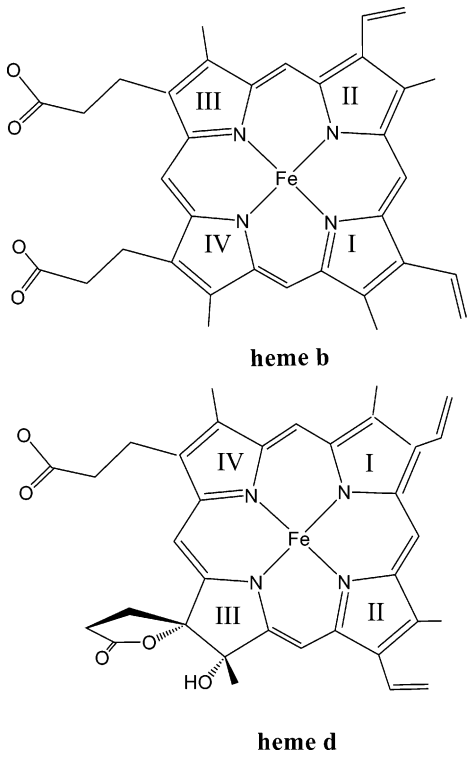

Figure 1. Structures of heme b and heme d.

Cpd I can explain the longer Fe−O distances found in some X-ray-determined Cpd I structures. For example, horseradish peroxidase Cpd I was found to be particularly radiation sensitive, with a third of it being converted to Cpd II after collection of just 8 degrees of data.[8] However, the propensity for reduction to Cpd II varies considerably among catalases. Cpd I of heme d-containing catalases[34] (Figure 1) apparently are not reduced by ferrocyanide treatment, whereas Cpd I of heme b-containing catalases such as BLC are converted easily to Cpd II[34] under the same conditions. Therefore, if either the presence of Cpd I* or the reduction of Cpd I to Cpd II is the major explanation of longer Fe−O bond lengths, the heme d-containing catalases may be found with predominantly short Fe−O bond lengths. For heme b-containing enzymes the outcome may vary depending upon the differences in the ease of Cpd I* or Cpd II production and the experimental conditions for diffraction data collection.

The lack of high-resolution structures of oxidized catalase intermediates makes it difficult to verify these predictions. The only structure reported for catalase Cpd I is that of PMC[33] which shows a refined Fe−O distance of 1.76 Å, intermediate between a Fe═O double bond and a Fe−OH single bond. Unfortunately, the low resolution of 2.5 Å and use of restraints precludes drawing firm conclusions. The 2.0 Å structure of MLC after oxidation with peroxoacetic acid exhibits a Fe−O bond length of 1.87 Å,[28] indicative of a hydroxoferryl group, and this was attributed to the formation of Cpd II. Nevertheless, the apparent conversion of Cpd I to Cpd II in MLC occurred spontaneously in the absence of added reducing agent and before exposure to X-rays, suggesting that Cpd I* and not Cpd II was present in the sample. Within the framework of our structure and function studies of catalases, we report here the structure of oxidized catalase intermediates generated by peroxoacetic acid treatment of heme b-containing HPC and heme d-containing PVC at 1.8 and 1.7 Å resolution, respectively. Interpretation of the structures is complemented by QM/MM density functional theory calculations with the objectives of (i) helping to assign a protonation state of the active site and (ii) elucidating the electronic changes caused by the heme modification (Figure 1).

Experimental Section

Crystallization and Data Treatment of HPC. The HPC protein analyzed in this work was expressed from plasmid pSO100[35] in the catalase deficient *E. coli* UM255.[36] Crystallization was as previously described[37] at room temperature by the vapor diffusion hanging-drop method at a protein concentration of about 6 mg/mL over a reservoir containing 15% PEG MME 550, 0.1 M sodium citrate pH 5.6, 10 mM $ZnSO_4$. Before flash cooling in liquid nitrogen the crystals were soaked for 1 to 2 min at 20 °C in a solution of the cocrystallization buffer, pH 5.6, supplemented with 100 mM peroxoacetic acid. During soaking, the HPC crystals changed from brown to red in color within seconds (Figure S1 of the Supporting Information), indicative of a reaction intermediate being formed. After a 2 min soak, the crystal was flash cooled and kept at 100 K, and diffraction data were collected using synchrotron radiation at the BM16 beam line (Grenoble, France) at a wavelength of 0.97 Å. As before, crystals were orthorhombic, space group $P2_12_12$ with two subunits in the crystal asymmetric unit. Diffraction data were obtained from crystals cooled with a nitrogen cryo-stream giving unit cell parameters of $a = 64.3$, $b = 154.5$, and $c = 95.8$ Å and $\alpha, \beta, \gamma = 90.0^{\circ}$. The diffraction data set was processed using the program MOSFLM[38] and scaled with the program SCALA.[39] There was 5% of the measured reflections in every data set reserved for R_{free} monitoring during automatic refinement (Table 2). Structure determination was carried out with the program MOLREP[40] using the native HPC structure as the searching model. Refinements were

(34) (a) Kikuchi-Torii, K.; Hayashi, S.; Nakamoto, H.; Nakamura, S. *J. Biochem.* **1982**, *92*, 1449−1456. (b) Obinger, C.; Maj, M.; Nicholls, P.; Loewen, P. C. *Arch. Biochem. Biophys.* **1997**, *342*, 58−67. (c) Chelikani, P.; Carpena, X.; Perez-Luque, R.; Donald, L. J.; Duckworth, H. W.; Switala, J.; Fita, I.; Loewen, P. C. *Biochemistry* **2005**, *44*, 5597−5605.

(35) Odenbreit, S.; Wieland, B.; Haas, R. *J. Bacteriol.* **1996**, *178*, 6960−6967.
(36) Switala, J.; Loewen, P. C. *Arch. Biochem. Biophys.* **2002**, *401*, 145−154.
(37) Loewen, P. C.; Carpena, X.; Rovira, C.; Ivancich, A.; Perez-Luque, R.; Haas, R.; Odenbreit, S.; Nicholls, P.; Fita, I. *Biochemistry* **2004**, *43*, 3089−3103.
(38) Collaborative Computational Project, Number 4. *Acta Crystallogr.* **1994**, *A50*, 760−763.
(39) Evans, P. R. Scala. *Joint CCP4 ESF-EACBM Newsl.* **1997**, *33*, 22−24.
(40) Vagin, A.; Teplyakov, A. *J. Appl. Cryst.* **1997**, *30*, 1022−1025.

Table 2. Data Collection and Structural Refinement Statistics for Cpd I* of HPC and Cpd I of PVC

	HPC	PVC
Data Collection Statistics		
space group	$P2_12_12$	$P3_121$
unit cell params		
a (Å)	64.4	142.4
b (Å)	154.3	142.4
c (Å)	95.8	132.2
α, β, γ (deg)	90, 90, 90	90, 90, 120
resolution (Å)	37−1.86 (1.86−1.95)[a]	20−1.71 (1.73−1.71)[a]
unique reflns	80 997 (11 375)	164 651 (5381)
completeness (%)	97.4 (97.4)	98.1 (64.7)
R_{sym}[b]	0.084 (0.40)	0.068 (0.29)
$<I/\sigma I>$ (%)	6.4 (1.5)	15.5 (3.5)
multiplicity	4.1 (3.7)	3.3 (2.9)
Model Refinement Statistics		
No. of reflns	74 135	156 337
R_{cryst} (%)[c]	14.8	13.2
R_{free} (%)[d]	18.8	15.3
non-hydrogen atoms	9112	12 590
water molecules	884	1490
avg B-factor (Å^2)		
protein	16.53	14.91
prosthetic group	12.84	12.62
waters	24.15	25.24
est coordinate error (Å)[e]	0.08	0.05
rms deviations		
in bonds (Å)	0.015	0.016
in angles (deg)	1.55	1.57

[a] Values in parentheses correspond to the highest resolution shell. [b] $R_{sym} = \sum_{hkl}\sum_j|I_{hkl,j} - \langle I_{hkl}\rangle|/\sum_{hkl}\langle I_{hkl}\rangle$. [c] $R_{cryst} = \sum||F_{obs}| - |F_{calcd}||/\sum|F_{obs}|$. [d] R_{free} is as for R_{cryst} but calculated for a test set comprising reflections not used in the refinement. [e] Based on maximum likelihood

completed using the program REFMAC[41] in which all hydrogens were generated during refinement and manually processed with the graphics program O.[42]

Crystallization and Data Treatment of PVC. PVC was purified[43] and crystallized[44] as previously described by the hanging-drop vapor diffusion method against a precipitant solution of 38% MPD and 50 mM sodium acetate buffer pH 5.2. Droplets of 10 μL containing 25−30 mg mL^{-1} protein solution in the same buffer were mixed before crystallization with an equal volume of precipitant solution. Crystals belong to space group $P3_12_11$ and have unit cell dimensions $a = b =$ 144.4 and $c =$ 133.8 Å with two subunits of the tetramer molecule in the asymmetric unit. A PVC crystal was soaked for 2 min in a solution containing 125 mM peroxoacetic acid, 40% MPD, 1 mg/mL PVC, and 0.05 M sodium acetate pH 5.2. During soaking, the crystal changed in color from brown to green suggesting that Cpd I formation had occurred. After a 2 min soak, the crystal was flash cooled and kept at 100 K, and diffraction data were collected using synchrotron radiation at the BW7B beam line (EMBL, Hamburg) at a wavelength of 0.89 Å. The peroxoacetic acid soak solution was prepared by adjusting the pH to 5.2 with a small amount NaOH and adding 1 mg/mL of PVC to remove any hydrogen peroxide present in the peroxoacetic acid. Data were processed using DENZO and SCALEPACK.[45] The model of native PVC[44] was used as the starting model for refinement using REFMAC[42] and manually processed with the graphics program O.[42] Data collection and refinement statistics are provided in Table 2.

Structure factors and coordinates have been submitted to the protein data bank as 2IQF for HPC Cpd I and 2IUF for PVC Cpd I. Figures were prepared using either SETOR[46] or VMD.[47]

Spectroscopic Analysis. Solutions of 5 μM HPC, PVC, or BLC were treated in 0.1 M sodium citrate buffer pH 5.6 with 1 mM peroxoacetic acid for 1 min at 20 °C. Absorption spectra were obtained using a Milton Roy MR3000 diode array spectrophotometer. A fresh solution of 100 mM peroxoacetic acid was pretreated with 4 μM BLC for 1 h to remove any H_2O_2 prior to a 1:100 dilution with the three enzymes.

Force-Field MD Simulations. Before starting the QM/MM simulations, a classical molecular dynamics simulation was performed to equilibrate tetrameric HPC and a truncated form of PVC lacking the C-terminal flavodoxin-like domain in each of the four subunits. For protein residues, the Cornell et al. force-field,[48] as implemented in the AMBER 7.0 program,[49] was used. For heme b in HPC, the parameters of Banci et al. were used,[50] and for the *cis*-hydroxy-γ-spirolactone heme d in PVC the parameters from GAFF in the AMBER package were used.[49] A renormalization of the charges is needed to reproduce the formal oxidation states of the iron atom (+4) and the ligands (−1 and −2 for the porphyrin in Cpds I and II, respectively; −2 for the axial oxygen atom of the oxoferryl unit; and −1 for the OH ligand). For oxidized heme b, the charges reported previously for a heme b based Cpd I were used.[51] In the case of heme d, the charges were obtained from a CPMD gas-phase calculation of the prosthetic group and the proximal tyrosinate and arginine. Conventional (pH = 7) protonation states were chosen for all residues. The protonation state of the histidine residues took into account their hydrogen bond environment, and all aspartates and glutamates were taken as deprotonated to carboxylate anion, except when there was a close contact between two acidic residues. The proximal tyrosines (339 in HPC and 351 in PVC) were taken as deprotonated. Four sodium ions per subunit of HPC and seven per subunit of PVC were added to achieve neutrality of the protein structure. The system was enveloped in a box of equilibrated TIP3P water molecules with volume 104 Å × 119 Å × 121 Å for HPC and 120 Å × 119 Å × 144 Å for PVC. The total size of the system is 128856/178558 atoms, respectively, (31856/32443 protein and heme atoms + 97000/146115 water and counterion atoms). The system was equilibrated in several steps. First, all water molecules and counterions were relaxed with a gradient minimizer, and then the protein was also minimized. Because of the enormous size of the protein, only the first subunit was allowed to move, and the other three were fixed. Next, the solvent was equilibrated for 40/80 ps at 150 K (protein constrained), and again the first subunit was equilibrated at the same temperature for another 40/80 ps. Once the whole system was at 150 K, it was equilibrated at 300 K for 280/233 ps, again coupling a bath to achieve the desired temperature. The simulation was continued for about one nanosecond at constant pressure, allowing the cell volume to evolve until equilibration. The structure after MD simulation did not change significantly with respect to the initial X-ray structure. Analysis of the trajectories was carried out using standard tools of AMBER.[49]

Hybrid QM/MM Calculations. Once the system was equilibrated, QM/MM simulations were initiated. Because of the enormous size of the protein, the calculations were performed on a reduced model consisting of all residues within 20 Å from the heme iron. This corresponds to a sizable protein fragment (4141 and 4986 atoms,

(41) Murshudov, G. N.; Vagin, A. A.; Dodson, E. J. *Acta Crystallogr., Sect. D: Biol. Crtystallogr.* **1997**, *53*, 240−255.
(42) Jones, T. A.; Zou, J. Y.; Cowan, S. W.; Kjeldgaard, M. *Acta Crystallogr., Sect. A: Found. Crystallogr.* **1991**, *47*, 110−119.
(43) Gulyi, M. F.; Gudkova, L. V.; Degtyarj, R. G.; Mironenko, N. I.; Latyshko, N. V. *Dokl. Akad. Nauk SSSR* **1975**, *225*, 211−213.
(44) Vainshtein, B. K.; Melik-Adamyan, W. R.; Barynin, V. V.; Vagin, A. A.; Grebenko, A. I.; Borisov, V. V.; Bartels, K. S.; Fita, I.; Rossmann, M. G. *J. Mol. Biol.* **1986**, *188*, 49−61.
(45) Otwinowski, Z.; Minor, W. *Methods Enzymol.* **1997**, *276*, 307−326.
(46) Evans, S. *J. Mol. Graphics* **1993**, *11*, 134−138.
(47) Humphrey, W.; Dalke, A.; Schulten, K. *J. Mol. Graphics* **1996**, *14*, 33−38.
(48) Cornell, W. D.; Cieplak, P.; Bayly, C. I.; Gould, I. R.; Merz, K. M., Jr.; Ferguson, D. M.; Spellmeyer, D. C.; Fox, T.; Caldwell, J. W.; Kollman, P. A. *J. Am. Chem. Soc.* **1995**, *117*, 5179−5197.
(49) Pearlman, D. A.; Case, D. A.; Caldwell, J. W.; Ross, W. S.; Cheatham, T. E.; Debolt, S.; Ferguson, D.; Seibel, G.; and Kollman, P. *Comput. Phys. Commun.* **1995**, *91*, 1−41.
(50) Banci, L.; Gori-Savellini, G.; Turano, P. *Eur. J. Biochem.* **1997**, *249*, 716.
(51) (a) Collins, J. R.; Camper, D. L.; Loew, G. H. *J. Am. Chem. Soc.* **1991**, *113*, 2736−2743. (b) Harris, D.; Loew, G. *J. Am. Chem. Soc.* **1995**, *117*, 2738−2746.

Scheme 1

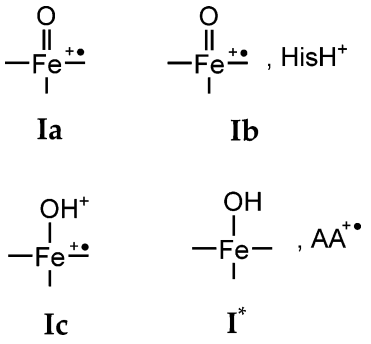

respectively, in HPC and PVC) and it is expected to account for all the relevant heme−protein interactions affecting the electronic structure at the active center. Figure S2 (Supporting Information) shows the QM/MM partition used in the calculation which included the iron−porphyrin with its methyl and vinyl groups and the *cis*-hydroxy-γ-spirolactone in heme d, the phenolate side chain of the proximal Tyr339/351, and the methylguanidinium side chain of Arg335/347, which is hydrogen bonded to the phenolate oxygen atom of Tyr339/351. Previous work demonstrated that both Tyr339/351 and Arg335/347 influence significantly the structure and ligand properties of the heme.[52] On the distal side of the heme, the catalytic residues (Asn129/137 and His56/64, modeled by methylimidazole and ethylamide, respectively), the water molecule coordinated by histidine and asparagine, and the side chain of Ser95/103, which interacts with its N_δ-H of His56/64, were included. Two additional conserved water molecules hydrogen bonded to the distal residues Asn129/137 and Ser95/103 were also included. The rest of the system was treated with the AMBER force field.[49]

Four different configurations for the heme−ligand bonds were considered (Scheme 1). The first was the traditional oxoferryl configuration ($Por^{\bullet+}-Fe^{IV}=O$) which corresponds to a neutral system with a total spin $S = {}^3/_2$, labeled **Ia**. The second and third were two protonated forms of **Ia**, $Por^{\bullet+}-Fe^{IV}=O\cdots His-H^+$, labeled **Ib**, and $Por^{\bullet+}-Fe^{IV}-OH^+$, labeled **Ic**. The total spin of these systems is the same as in **Ia** ($S = {}^3/_2$), but they bear a positive charge in the form of a proton either on the distal histidine or on the oxo ligand. Finally, the system resulting from migration of the radical to the protein ($Por-Fe^{IV}-OH$, $AA^{\bullet(+)}$) was considered, but the huge QM region covering all tyrosine and tryptophan residues close to the heme was beyond our computational capabilities. However, as mentioned in the introduction, $Por-Fe^{IV}-OH$, $AA^{\bullet(+)}$, is isoelectronic with Cpd II on the hydroxoferryl heme. Therefore, we modeled this intermediate using the same active-site electronic state as for Cpd II (i.e., a triplet spin state). Protonation of the oxoferryl unit was considered since Cpd II is generally assumed to be protonated at neutral pH.[9,10,14] As mentioned in the introduction, we use the notation **I*** to refer to the $Por-Fe^{IV}-OH$, $AA^{\bullet(+)}$ intermediate, since there are two oxidation equivalents missing from the protein−heme unit, the same as in Cpd I. Hybrid QM/MM optimizations, with no symmetry constraints, were performed for each of the four species **Ia**, **Ib**, **Ic**, and **I***. The method developed by Laio, VandeVondele, and Röthlisberger[53] combining the first principles molecular dynamics method of Car and Parrinello (CPMD)[54] with a force-field molecular dynamics methodology (i.e., QM/MM CPMD) was used. Previous work has demonstrated the reliability of the QM/MM CPMD method in the description of structural, energetic, and dynamic properties of systems of biological interest, including hemeproteins.[10,52,55] In this approach, the system is partitioned into a QM fragment and a MM fragment. The dynamics of the atoms on the QM fragment depend on the electronic density, $\rho(r)$, computed with DFT, while the dynamics of the atoms on the MM fragment are ruled by an empirical force field. The QM−MM interface is modeled by the use of a link atom pseudopotential that saturates the QM region.[56] Seven link atoms were used, located at Asn129/137, His56/64, Ser95/103, Tyr339/351, Arg335/347, and the two heme b or the one heme d propionates (Figure S2 of the Supporting Information). The electrostatic interactions between the QM and MM regions are handled via a fully Hamiltonian coupling scheme[53] where the short-range electrostatic interactions between the QM and the MM regions are explicitly taken into account for all atoms. An appropriately modified Coulomb potential was used to ensure that no unphysical escape of the electronic density from the QM to the MM region occurs. The electrostatic interactions with the more distant MM atoms are treated via a multipole expansion. Bonded and van der Waals interactions between the QM and the MM region are treated with the standard AMBER force field.[49] Long-range electrostatic interactions between MM atoms have been described with P3M implementation[57] using a $64 \times 64 \times 64$ mesh. The Kohn−Sham orbitals were expanded in a plane wave basis set with the kinetic energy cutoff of 70 Ry. Ab initio pseudopotentials, generated within the Troullier−Martins scheme,[58] were used. Two types of pseudopotentials for the iron atom were tested for the $Por^{\bullet+}-Fe^{IV}=O$, $Por^{\bullet+}-Fe^{IV}-OH^+$ and $Por-Fe^{IV}-OH$ systems in HPC: the eight valence electrons pseudopotential already used in previous works[10,52,59] supplemented with nonlinear core corrections (NLCC)[60] and a 16 valence electrons pseudopotential. Only slight changes in the Fe=O and $Fe-O_{Tyr}$ distances were found (± 0.02, and ± 0.03 Å, respectively), and the same trends were observed. Therefore we used the eight valence electrons pseudopotential with NLCC for all systems. The calculations were made using the generalized gradient-corrected approximation of the spin-dependent density functional theory (DFT-LSD), following the prescription of Becke and Perdew.[61] The QM system was enclosed in an isolated supercell of size $15341 \times 21160 \times 20102$ Å^3/$22483 \times 18780 \times 18515$ Å.^{3} Structural optimizations of all reaction intermediates (Scheme 1) were performed by means of molecular dynamics with annealing of the atomic velocities, until the maximum component of the nuclear was lower than 10×10^{-05} au. Short CPMD simulations (1 ps) for the oxoferryl forms (PVC-**Ia** and HPC-**Ia**) were performed to analyze the changes in the spatial distribution of the spin density owing to the thermal motion. A time step of 0.12 fs and a fictitious electronic mass of the CP Lagrangian of 700 au were used. Further details on the QM/MM methodology used here can be found in ref 53.

It might be argued that the use of the QM/MM methodology for this problem could be avoided, because the Fe−O distances are already well reproduced using small iron−porphyrin models.[9−11,13−5a,31,32] In fact, large active site models are often used with success to study enzymatic reaction cycles.[62] In our case, however, this was found not to be the case. Test calculations in some of the species considered (e.g., PVC-**Ia** and PVC-**Ib**) using a large QM model (equivalent to the QM subsystem used for the QM/MM calculation) showed that the distance

(52) Rovira, C.; Fita, I. *J. Phys. Chem. B* **2003**, *107*, 5300−5305.
(53) Laio, A.; vandeVondele, J.; Röthlisberger, U. *J. Chem. Phys.* **2002**, *116*, 6941−6947.
(54) (a) Car, R.; Parrinello, M. *Phys. Rev. Lett.* **1985**, *55*, 2471−2474. (b) Marx, D.; Hutter, J. Ab initio molecular dynamics: Theory and implementation. In *Modern Methods and Algorithms of Quantum Chemistry;* Grotendorst, J., Ed.; John von Neumann Institute for Computing: Julich, Germany, 2000; pp 301−409. (c) *CPMD program*; IBM Corp, MPI für Festkörperforschung: Stuttgart, 1990−2003; 1997−2001; URL: http://www.cpmd.org.
(55) See for instance: (a) Carloni, P.; Röthlisberger, U.; Parrinello, M. *Acc. Chem. Res.* **2002**, *35*, 455−464. (b) Ivanov, I.; Chen, B.; Raugei, S.; Klein, M. L. *J. Phys. Chem. B* **2006**, *110*, 6365−6371. (c) Papoian, G. A.; DeGrado, W. F.; Klein, M. L. *J. Am. Chem. Soc.* **2003**, *125*, 560−569. (d) Mordasini, T.; Curioni, A.; Andreoni, W. *J. Biol. Chem.* **2003**, *278*, 4381−4384. (e) Biarnés, X.; Nieto, J.; Planas, A.; Rovira, C. *J. Biol. Chem.* **2006**, *281*, 1432−1441.
(56) von Lilienfeld, O. A.; Tavernelli, I.; Rothlisberger, U.; Sebastiani, D. *J. Chem. Phys.* **2005**, *122*, 013133 (1−6).
(57) Hünenberger, P. *J. Chem. Phys.* **2000**, *113*, 10464−10476.
(58) Troullier, M.; Martins, J. L. *Phys. Rev. B* **1991**, *43*, 1993−2006.
(59) Rovira, C.; Kunc, K.; Hutter, J.; Ballone, P.; Parrinello. M. *J. Phys. Chem. A* **1997**, *101*, 8914−8925.
(60) Louie, S. G.; Froyen, S.; Cohen, M. L. *Phys. Rev. B* **1982**, *26*, 1738−1742.
(61) (a) Becke, A. D. *J. Chem. Phys.* **1986**, *84*, 4524−4529. (b) Perdew, J. P. *Phys. Rev. B.* **1986**, *33*, 8822−8824.
(62) Bassan, A.; Blomberg, M.; Borowski, T.; Siegbahn, P. E. M. *J. Inorg. Biochem.* **2006**, *100*, 727−743.

Table 3. Main Structural Parameters[a] Defining the Active-Site Structure of the Reaction Intermediates of HPC Defined in Scheme 1

parameter	X-ray[b]	Ia	Ib	Ic	I*
Fe−O	1.80/1.85	1.68	1.71	1.78	1.79
Fe−O_{Tyr}	1.95/1.92	2.14	2.05	1.99	2.00
O−O_{Tyr}	3.72/3.76	3.82	3.75	3.77	3.78
Fe−N_{porph}	2.03/2.06[c]	2.01−2.02	2.00−2.02	2.00−2.01	2.00−2.02
O···O_w	2.98/2.91	2.79	2.54	3.31	3.34
N_ϵ···O_w	2.71/2.74	2.89	2.63 (1.56)[d]	2.90	2.89
N_{Asn}···O_w	3.23/3.08	3.83	4.11	3.89	3.84
O···H_w		1.85	1.49	2.60	2.60
N_ϵ···H_w		1.88	3.32	1.89	1.88
N_ϵ···O	3.33/3.45	3.42	3.75 (3.16)[e]	3.41 (2.44)[f]	3.53 (2.59)[f]
NH_{Asn}···O_w		2.81	3.10	2.89	2.85
Fe···O_w	4.13/4.13	4.06	3.76	4.63	4.68
Fe out-of-plane	0.036/0.033	0.214	0.108	0.054	0.058
O−H				0.99	0.99
∠Fe−O−H			122.55[g]	109.39	107.83
∠O═Fe−O_{Tyr}	167.3/169.5	177.0	173.83	174.26	174.74
∠Fe−O_{Tyr}−C	128.7/126.7	127.5	122.08	124.00	124.59
H···O_{Tyr}		1.79/1.88	1.76/2.02	1.84/2.07	1.82/2.02
N_{Arg+}···O_{Tyr}	2.81/2.68[h]	2.77/2.81	2.77/2.92	2.84/2.97	2.82/2.93

[a] Distances are given in angstrom and angles in degrees. [b] Values corresponding to the two independent protein subunits. [c] An average of the four Fe−N distances is given for each subunit. [d] The distance between the O_w and the proton on the His is given in parenthesis. [e] The distance between the oxoferryl oxygen and the proton on the His is given in parenthesis. [f] The distance between the proton on the hydroxoferryl oxygen and nitrogen of the His is given in parenthesis. [g] Fe═O···H^+(His) angle. [h] An average of the two N−O distances is given for each subunit.

Table 4. Main Structural Parameters[a] Defining the Active-Site Structure of the Reaction Intermediates of PVC Defined in Scheme 1

parameter	X-ray[b]	Ia	Ib	Ic	I*
Fe−O	1.72/1.72	1.69	1.70	1.80	1.80
Fe−O_{Tyr}	2.00/2.04	2.07	2.08	1.92	1.99
O--O_{Tyr}	3.72/3.76	3.36	3.76	3.74	3.79
Fe−N_{porph}	2.03/2.02[c]	2.01−2.06	2.01−2.06	2.00−2.05	2.01−2.04
O···O_w	3.27/3.30	2.87	2.58	2.94	2.96
N_ϵ···O_w	2.71/2.74	2.95	2.68 (1.65)[d]	2.92	2.80
N_{Asn}···O_w	3.25/3.20	5.03	4.69	5.06	4.70
O···H_w		1.88	1.54	1.96	1.98
N_ϵ···H_w		1.97	3.21	1.95	1.81
N_ϵ···O	3.37/3.43	4.26	3.99 (3.40)[e]	4.38 (5.07)[f]	4.35 (5.04)[f]
NH_{Asn}···O_w		4.03	3.71	4.05	3.68
Fe···O_w	4.29/4.32	4.30	3.93	4.52	4.47
Fe out-of-plane	0.091/0.113	0.091	0.110	0.052	0.043
O−H				0.99	0.99
∠Fe−O−H			123.96[g]	103.63	104.24
∠O═Fe−O_{Tyr}	175.55/175.58	174.97	179.23	178.03	177.46
∠Fe−O_{Tyr}−C	126.04/127.98	127.20	126.47	127.56	125.60
H···O_{Tyr}		1.93/1.96	1.95/2.03	1.98/2.10	1.98/1.99
N_{Arg+}···O_{Tyr}	2.82/2.83[h]	2.90/2.91	2.92/2.97	2.96/3.04	2.96/2.94

[a] Distances are given in angstrom and angles in degrees. [b] Values corresponding to the two independent protein subunits. [c] An average of the four Fe−N distances is given for each subunit. [d] The distance between the O_w and the proton on the His is given in parenthesis. [e] The distance between the oxoferryl oxygen and the proton on the His is given in parenthesis. [f] The distance between the proton on the hydroxoferryl oxygen and nitrogen of the His is given in parenthesis. [g] Fe═O···H^+(His) angle. [h] An average of the two N−O distances is given for each subunit.

between the distal His and its closest porphyrin pyrrole increases by 0.2 A from the QM/MM optimized distance (3.88 Å), increasing its deviation with respect to the X-ray structure (3.42−3.45 Å). As a consequence, the oxoferryl bond length is not affected by protonation of the His, unlike what is found in the QM/MM calculations (Tables 3 and 4). In addition, we found that the spin density on the distal His of PVC disappears (because of the decrease of the overlap between the imidazole ring of His64 and the porphyrin pyrrole), as well as the contribution of the Tyr351 oxygen (see later and Figure 8). Therefore, both the spin density distribution and the structure of PVC obtained with the QM model are qualitatively different from the one obtained using the QM/MM approach. This is in line with the recent QM/MM study of HRP by Derat et al.[32a] in which it was found that the protein environment accounts for most of the subtle features of Cpd I.

Results

Crystal Structures of HPC and PVC Treated with Peroxoacetic Acid. Treatment of HPC with peroxoacetic acid causes a change in the absorption spectrum consistent with the generation of Cpd II-like species (Figure 2a). This happens in the absence of an exogenous one-electron donor commonly used to convert Cpd I into Cpd II. For comparison, treatment of BLC with peroxoacetate produces a spectrum consistent with Cpd I formation (Figure 2c), and only with the subsequent addition of a one-electron donor, ferrocyanide, does a typical Cpd II spectrum appear (Figure 2c). The changes to the spectrum of the heme d-containing PVC (Figure 2b) caused by peroxoacetic acid are unlike those of the heme b-containing enzymes, but were similar to changes previously reported for the heme d-containing catalases from *E. coli* (HPII) and *A. niger* which had been interpreted as indicating conversion to Cpd I.[34] Furthermore, the absence of any subsequent spectral change on the addition of ferrocyanide was interpreted as indicating that heme d-containing catalases do not undergo conversion to Cpd II.[34]

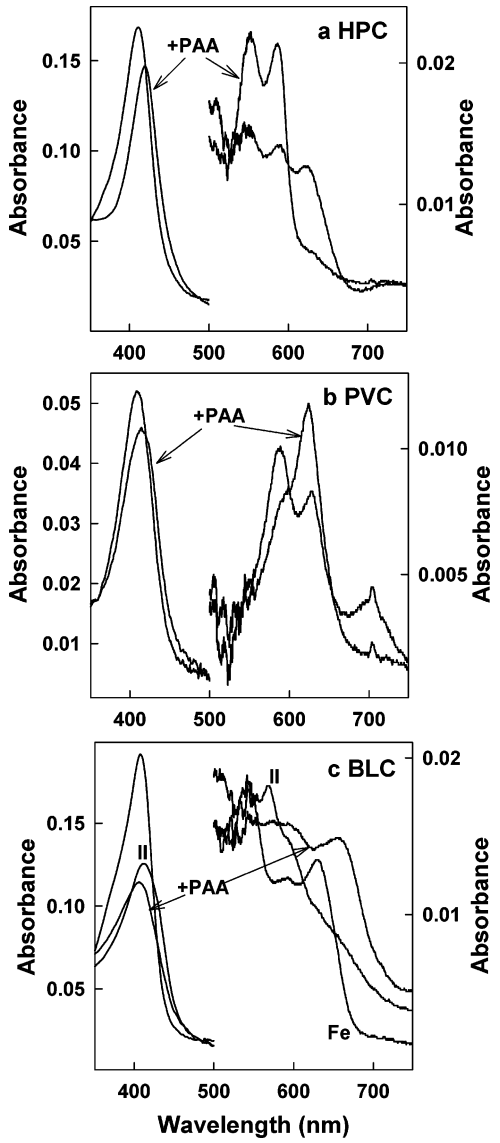

Figure 2. Changes in absorbance spectra of HPC (panel a), PVC (panel b), and BLC (panel c) caused by mixing with peroxoacetic acid. Spectra were determined before and 1 min after the addition of 1 mM peroxoacetic acid to a 5 μM solution of enzyme in 0.1 M sodium citrate buffer pH 5.6. In panel c, 8 μM potassium ferrocyanide was added 2 min after the addition of peroxoacetic acid to generate Cpd II and the spectrum determined after 5 min incubation. The left axis corresponds to 350−500 nm and the right axis corresponds to 501−750 nm.

The electron density map of HPC, a small subunit clade 3 catalase, treated with peroxoacetic acid is very similar to that of the native enzyme in defining main-chain and side-chain atoms of 982 amino acids and two heme groups in two subunits. The map shows clear continuity in both subunits over the complete length from Met1 to Lys491, with fourteen residues at the C-terminus predicted from the gene sequence being absent and presumed disordered. There is one significant area of change compared to the native enzyme, a region of continuous density extending from the heme iron in both subunits to a second atom that is best explained by formation of an oxoferryl or hydroxoferryl species (Figure 3a). Refinement with loose restraints on the iron−oxygen bond resulted in Fe−O bond lengths of 1.80 and 1.85 Å in the two subunits, which is longer than expected for an oxoferryl Fe═O double bond. However, the distance is similar to the Fe−O bond lengths observed in oxidized MLC,[28] CcP,[22a] and KatG.[23] By reducing the occupancy in subsequent rounds of refinement until the B factor of the oxygen became equivalent to that of the iron, the occupancy of the distal oxygen in HPC is estimated to be approximately 60%. This is either due to incomplete reaction or photoreduction back to the native enzyme (as commented in the introduction). The only other obvious changes resulting from the peroxoacetate soaking are the replacement of the single molecule of azide present in the native structure with a molecule of acetate and the oxidation of 4 of 10 methionines (residues 162, 181, 292, and 372) to methionine sulfoxide, in each subunit. One of the oxidized methionines, Met181, is located in the main channel leading to the heme and appears well preserved in catalases, while Met162 is accessible from the channel.

The structure of PVC, a large subunit clade 2 catalase, after treatment with peroxoacetic acid, is also similar to that of the native enzyme[63] but with some revision to take into account the recently reported protein sequence.[64] The present PVC structure defines main-chain and side-chain atoms of 1376 amino acids and 2 heme d groups in two subunits. The map shows clear continuity in both subunits over the complete length from residue 2 to 689. A region of continuous density extends from the heme iron in both subunits to a second atom that is best explained by formation of an oxoferryl or hydroxoferryl species (Figure 3b). Refinement with loose restraints on the iron−oxygen bond resulted in Fe−O bond lengths of 1.72 Å in the two subunits, which is close to the expected distances for an oxoferryl Fe═O double bond. Another obvious change is the oxidation of methionines 193, 254, 316, 463, and 569 to methionine sulfoxide in each subunit. There are also four acetate molecules introduced into the protein by the peroxoacetate soaking, primarily in the main channel leading to the heme but also one on the proximal side of the heme, and a clearly defined peroxoacetate molecule not far from the oxidized methionine Met193 in the main channel (Figure 4). The distribution of peroxoacetate and acetate molecules seems to confirm the role of the main channel leading to the heme as the primary access route, although the alternative lateral channel may provide access for the acetate on the proximal side of the heme.

Theoretical Calculations of HPC Intermediates: Optimized Structure and Electronic Properties. The main structural parameters describing the optimized structures of the four species considered, in comparison with the crystal structure data for oxidized HPC, are listed in Table 3. The structures of the primary oxoferryl porphyrin radical species (**Ia**), its histidine protonated (**Ib**), and its oxoferryl protonated (**Ic**) derivatives as well as the one-electron reduced hydroxoferryl protein radical form (**I***) are shown in Scheme 1. The overall structure of **Ia** (Figure 5a) is in reasonable agreement with the crystal structures, except for variations in the iron-axial ligand bond distances. The Fe−O distance (1.68 Å) is shorter than the experimental distances observed in HPC by 0.12 or 0.17 Å, depending on the protein subunit, and the Fe−O_{Tyr} distance (2.14 Å) is 0.19 or 0.22 Å longer than experimental (Table 3). These values are in agreement with previous calculations on heme models having similar axial ligation.[9−11,31] A single water is hydrogen bonded to His56, Asn129, and the oxoferryl oxygen, as it is found in

(63) Vainshtein, B. K.; Melik-Adamyan, W. R.; Barynin, V. V.; Vagin, A. A.; Grebenko, A. I. *Nature (London)* **1981**, *293*, 411−412.
(64) Kozlov, E. A.; Levitina, T. L.; Bobrovskaj, M. T.; Ovander, M. N.; Gudkova, L. V.; Latyshko, N. V. *Biopolim. Klitina* **2001**, *17*, 283−291.

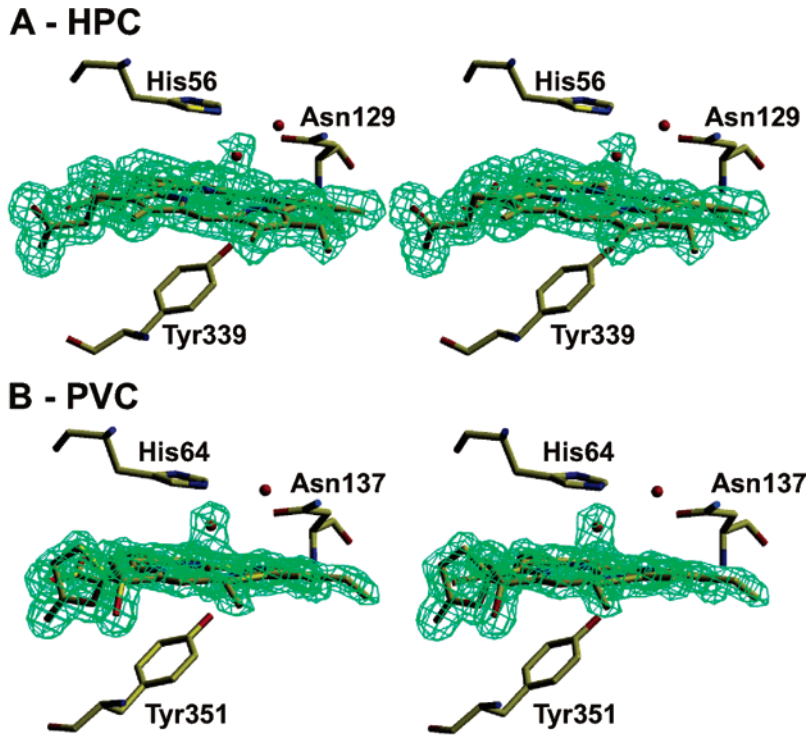

Figure 3. Stereoviews of the structures of HPC (a) and PVC (b) soaked with peroxoacetic acid. The F_o-F_c omit electron density maps of the heme cavity calculated using a model lacking the heme and distal ligand oxygen residues drawn at $\sigma = 3.0$ are drawn in green.

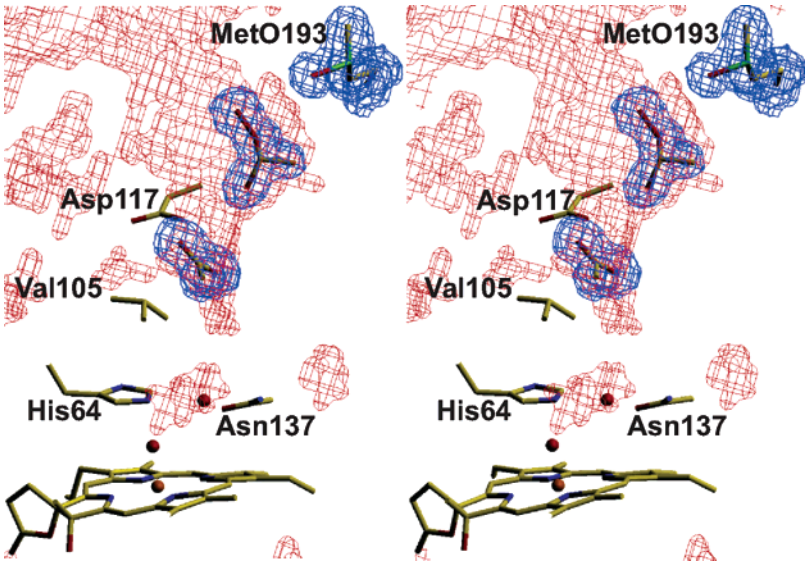

Figure 4. Stereoview of the main channel leading to the heme pocket and the heme pocket in oxidized PVC. The $2F_o-F_c$ electron density map drawn at $\sigma = 1.0$ of the methionine sulfoxide at residue 193, an acetate, and a peracetate in the channel is drawn in blue. The proximity of the carboxylate groups of Asp117 and the acetate molecule suggests the presence of the acidic form. Oxidation of methionine residues lining the main heme channel, a conserved feature, might have a functional role in catalases. The surface representation of the channel calculated in VOIDOO[74] is drawn in red.

the experimental structure. Most likely, the network of hydrogen-bond interactions connecting the histidine N_δ with one heme propionate (through Ser95) makes the His-N_ϵ atom a very good proton acceptor. As a consequence, the hydrogen-bond distance between His56 and the pocket water is shorter than the distance between the water and the Asn129 residue.

Protonation of the distal histidine (**Ib**) lengthens slightly the Fe═O bond (from 1.68 to 1.71 Å), but the distance is still much shorter than that observed in the crystal structure (1.80/1.85 Å) suggesting that the oxoferryl structure is not present in the crystal. When the oxoferryl moiety is protonated (**Ic**), the Fe−O distance increases significantly to 1.78 Å, reflecting the change from a double to a single Fe−O bond. At the same time, the Fe−O_{Tyr} distance decreases from 2.14 to 1.99 Å. Protonation is expected to reinforce this bond because most of the electron density of the Fe atom in the $Por^{\bullet+}-Fe^{IV}$═O species **Ia** and **Ib** is used in the double bond with the distal oxygen (i.e., the orbital composed of the σ orbitals of O and O_{Tyr} and Fe{dz^2} is more polarized toward the O atom), reducing the density available for the single Fe−O_{Tyr} bond. Similar changes have previously

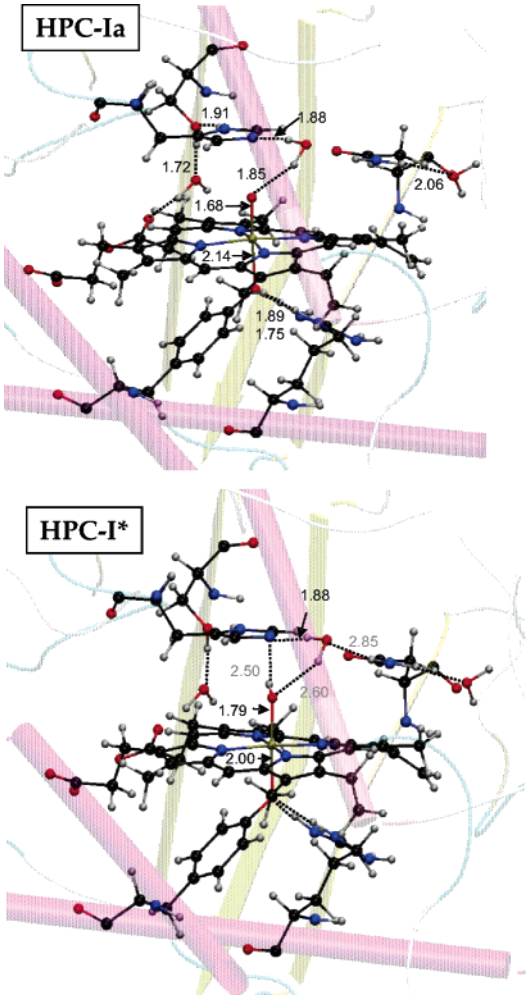

Figure 5. Optimized structures of the oxoferryl form, $Por^{\bullet+}-Fe^{IV}=O$ (**Ia**) and hydroxoferryl form, $Por-Fe^{IV}-OH$ (**I***) of HPC.

been observed in calculations of Cpd II, where the $Fe-O_{Tyr}$ distance shortens and the bond gets stronger upon protonation of the oxoferryl moiety.[10]

The structure of the one-electron reduced species, **I*** (Figure 5b) is similar to **Ic**, and the Fe−O distance (1.79 Å) is close to that observed in the crystal (1.80 and 1.85 Å) and clearly longer than an oxoferryl bond (1.68 Å). At the same time, the $Fe-O_{Tyr}$ distance decreases to 2.00 Å, in better agreement with the experimental values (1.95 and 1.92 Å). From the point of view of structure, both **Ic** and **I*** are good candidates to be the species present in the crystal structure of oxidized HPC.

The localization of the unpaired electrons of the species **Ia**, **Ib**, **Ic**, and **I*** was investigated by analyzing their spin-density distributions. The spin density on the porphyrin for a perfect D_{4h} Fe−porphyrin−O system has been often discussed in terms of originating from a half-filled orbital of A_{1u} or A_{2u} symmetry (Figure 6).[65] Early calculations of the oxoferryl form of Cpd I of several heme-containing proteins in the gas phase[66] performed on simplified models showed that the spin density has A_{2u} symmetry. However, in reality Cpd I is not symmetric, with the porphyrin showing a large degree of deformation from

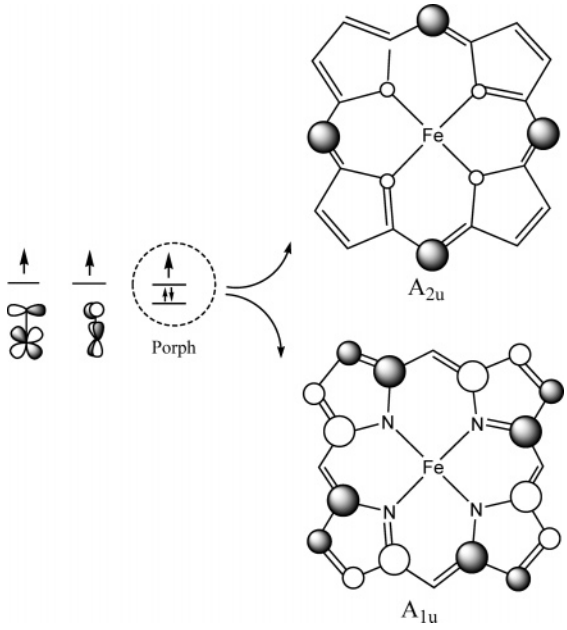

Figure 6. Schematic picture of the main molecular orbitals contributing to the spin density of Cpd I of heme-containing proteins for an ideal porphyrin complex of D_{4h} symmetry.

planarity (Figure 3), and both orbitals are allowed to mix. The spin densities of the oxoferryl species (**Ia** and **Ib**) are very similar, being concentrated on Fe=O and showing a large delocalization on the porphyrin ring, consistent with a porphyrin radical character (Figure 6). There is also a small fraction of spin density on the atom that is covalently attached to the proximal ligand (the tyrosinate oxygen) similar to what was observed for P450 Cpd I.[67] The total integrated spin density is 2.1 electrons on Fe=O and 0.9 electrons on the porphyrin + Tyr. The spatial symmetry of the spin density on the porphyrin reflects a mixture of A_{1u} (density on α and β pyrrole carbon atoms) and A_{2u} (density on the pyrrole nitrogen and meso carbon atoms), with more weight on the A_{2u} contribution. It is worth mentioning that a similar situation has been reported for Cpd I of horseradish peroxidase (HRP) using QM/MM calculations,[32a] suggesting that the spatial symmetry of the unpaired electrons in Cpd I is not strongly affected by the different axial ligands, a tyrosinate in catalase or histidine in peroxidase. The spin densities of **Ib** and **Ic** are similar to **Ia** but the spatial symmetry of the porphyrin density is more weighted on A_{1u} than A_{2u}, resulting in a change in the spin-density distribution on the porphyrin ring if $Por^{\bullet+}-Fe^{IV}=O$ is protonated. The spin-density distribution of **I*** (Figure 7b) shows that, as expected, the porphyrin radical disappears and the spin density is fully localized on the Fe−OH moiety, with a small contribution from the tyrosinate oxygen atom.

Theoretical Calculations of PVC Intermediates: Optimized Structure and Electronic Properties. The main structural parameters describing the optimized structures of the four species of PVC considered (**Ia**, **Ib**, **Ic**, and **I***) are compared with the crystal structure data in Table 4. The structure of the oxoferryl forms, **Ia** and **Ib** (Fe−O = 1.69/1.70 A, respectively), are in good agreement with the crystal structure in which the

(65) Hirao, H.; Shaik, S.; Kozlowski, P. M. *J. Phys. Chem. A* **2006**, *110*, 6091−6099.
(66) (a) Ghosh, A.; Almlof, J.; Que, L. *J. Phys. Chem.* **1994**, *98*, 5576−5579. (b) Kuramochi, H.; Noodleman, L.; Case, D. A. *J. Am. Chem. Soc.* **1997**, *119*, 11442−11451.
(67) See for instance: (a) Shaik, S.; Kumar, D.; de Visser, S. P.; Altun, A.; Thiel, W. *Chem. Rev.* **2005**, *105*, 2279−2328. (b) Bathelt, C. M.; Zurek, J.; Mulholland, A. J.; Harvey, J. N. *J. Am. Chem. Soc.* **2005**, *127*, 12900−12908.

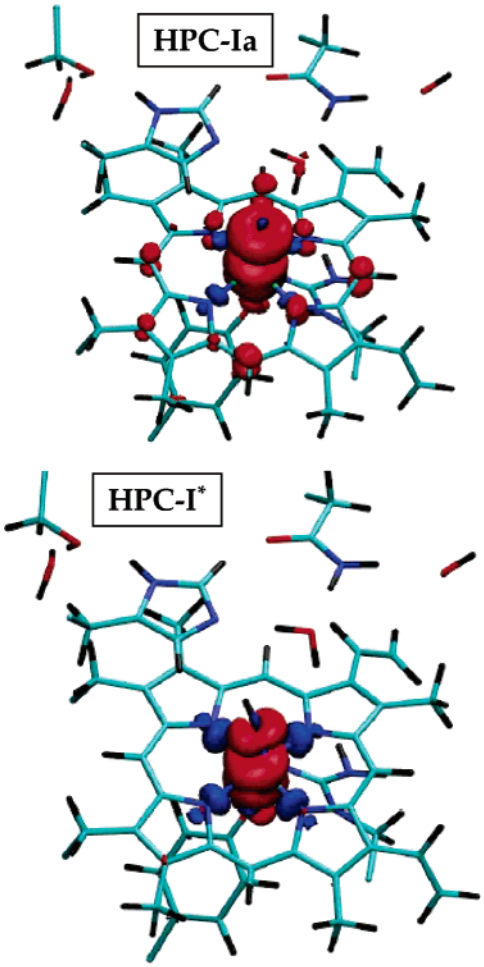

Figure 7. Spin-density distributions of the oxoferryl form, $Por^{\bullet+}-Fe^{IV}=O$ (**Ia**) and hydroxoferryl form, $Por-Fe^{IV}-OH$ (**I***) of HPC.

Fe−O bond length is 1.72 Å and the Fe−O_{Tyr} distance of 2.00/2.04 Å is slightly shorter than the calculated distances of 2.07 or 2.08 Å (Table 4). The single water in the heme pocket is again coordinated between the active site residues His64 and Asn137 as in the experimental structure. The Fe−O distances of the hydroxoferryl forms **Ic** and **I*** (1.80 Å) deviate considerably from the experimental value (1.72 Å). Therefore, the crystal structure of oxidized PVC is compatible with the oxoferryl porphyrin form.

In general, the active site structures calculated for **Ia**, **Ib**, **Ic**, and **I*** of PVC are similar to their HPC counterparts, and the small differences are a result of the spirolactone modification and extra hydroxyl group on ring III of heme d in PVC. The modifications result in the $C_{2D}-C_{3D}$ bond length in heme d being 0.21 Å longer than in heme b (1.56 compared to 1.35 Å), a result of the change from a $C_{sp^2}-C_{sp^2}$ to a $C_{sp^3}-C_{sp^3}$ bonding (see Figure 1). A second difference lies in the orientation of the hydroxyl ligand in the hydroxoferryl forms (**Ic** and **I***) which for HPC is projected toward the pyrrole ring III and the distal His (Figure 5b), whereas in PVC it is projected in opposite direction away from the distal His.

The spin density in the primary species **Ia** of PVC is concentrated on the Fe=O (Figure 8b) as in HPC, but the third unpaired spin shows a different distribution. It is not only delocalized over the porphyrin but also onto the distal histidine and to a lesser extent onto the O_{Tyr} and phenolate ring of the

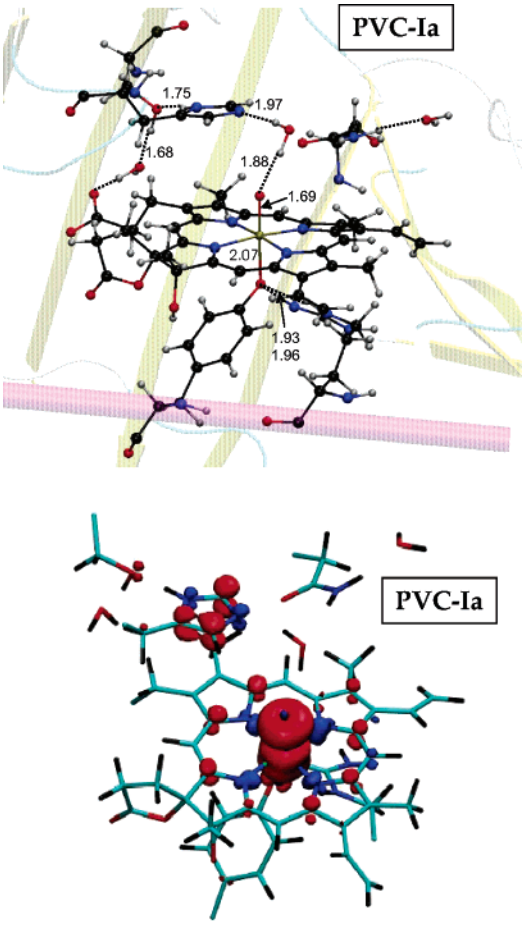

Figure 8. (a) Optimized structure of the oxoferryl form, $Por^{\bullet+}-Fe^{IV}=O$ (**Ia**) of PVC and (b) spin density distribution of **Ia**.

proximal ligand. Interestingly, the spatial symmetry of the spin density on the porphyrin reflects a mixture of A_{1u} (density on α and β pyrrole carbon atoms) and A_{2u} (density on the pyrrole nitrogen and meso carbon atoms), but unlike HPC it is more weighted to A_{1u}. Therefore, the spatial symmetry of the unpaired electrons in Cpd I depends on the type of heme group (heme b in HPC or heme d in PVC).

To analyze whether the spin density is affected by small structural changes in the active site, short molecular dynamics simulations at room temperature were performed, starting from the optimized structures. For HPC-**Ia**, the shape of the spin density (Figure 7a) does not change significantly during the dynamics, maintaining the A_{2u}-like symmetry of the unpaired spin on the porphyrin, whereas the spin density of PVC-**Ia** fluctuates between the porphyrin and distal His with different weights during the dynamics (Figure S3). In addition, increases in the spin density on the proximal tyrosine are evident in some snapshots of the molecular dynamics. Interactions between the hydroxyl group of the heme d modification and the phenolate ring of the tyrosine residue (O−H···π) are also observed during the dynamics.[68] The spin-density distribution of the His-protonated form, **Ib**, exhibits similar features to those of **Ia**, but the spin density evident on the histidine in PVC-**Ia** disappears. Partial protonation of His to produce PVC-**Ib** results in the main contribution to the spin density being from the porphyrin A_{2u} orbital, with only small participation of the distal

(68) Steiner, T. *Biophys. Chem.* **2002**, *95*, 195−201.

imidazole and the proximal tyrosinate. In summary, our results indicate that while the oxoferryl Cpd I species of HPC has an A_{2u}-like porphyrin radical, PVC has a porphyrin radical when the active site histidine is protonated (i.e., under the experimental conditions of the X-ray structure), and a "fluctuating" radical is partially delocalized on the distal histidine, the porphyrin and, to a lesser extent, the proximal tyrosine in the absence of histidine protonation (i.e., at higher pH).

Discussion

The structure and electronic configuration of the oxidized heme intermediates, commonly referred to as compounds I and II, formed as part of the catalytic cycle in catalases, peroxidases, and P450 have been the focus of considerable recent interest.[8−15,27,31,32,67,69,70] Prior to this report, the structures of one oxidized catalase, one oxidized catalase-peroxidase, and two oxidized peroxidase structures had been reported at a resolution sufficiently high to draw conclusions about the oxygen−iron covalent structure (Table 1). During the soaking of MLC with peroxoacetic acid, the spontaneous transformation of Cpd I was noted by color changes from brown to green to red of the crystal and spectral changes. Moreover a Fe−O bond length of 1.87 Å was observed.[28] This is consistent with reduction of the porphyrin radical by transfer of an electron from the protein resulting in the formation of a protein radical, similar to what was observed in BLC.[18] The formation of protein-based radical intermediate(s) in both MLC and HPC have been also detected by multifrequency EPR spectroscopy.[71] A similar process seems to have occurred in HPC where Fe−O bond lengths of 1.80 and 1.85 Å are observed, as well as in CCP and BpKatG.[22a,23] By contrast, only HRP,[8] and PVC, exhibit short 1.7 and 1.72 Å Fe−O bond lengths after oxidation with peroxoacetic acid. Therefore, the generalization that the presence of a porphyrin radical is associated with a short Fe−O bond whereas migration of the porphyrin radical to the protein leads to protonation and thus lengthening of the Fe−O is supported both experimentally and by QM/MM density functional theory calculations on the HPC and PVC structures. The calculated iron−ligand distance (Tables 3 and 4) for the $Por^{\bullet+}-Fe^{IV}=O$ models of 1.68 (HPC-**Ia**) and 1.69 Å (PVC-**Ia**) agree only with the PVC-**I** experimental bond length (1.72 Å). Given the acidic crystallization conditions (pH 5.6 for HPC and pH 5.2 for PVC) and assuming the pK_a of the distal histidine is similar to that reported in HRP Cpd I (5.0),[72] partial protonation of the distal histidine is likely. Therefore, because the calculated bond lengths are increased by only 0.01 or 0.02 Å as a result of histidine protonation, species **Ib** is also a candidate for the crystal structure of PVC.

The calculated Fe−O bond lengths in the oxoferryl protonated form Cpd Ic ($Por^{\bullet+}-Fe^{IV}-OH^{+}$), are 1.78−1.80 Å, very close to the bond lengths in the crystal structure of HPC. However, oxoferryl protonation and accumulation of **Ic** is unlikely because (i) the low pK_a for the oxoferryl group associated with a positively charged porphyrin radical would cause a rapid transfer of the proton from the oxoferryl group to the histidine via the water in the heme pocket, creating species **Ib** and (ii) there is no signature of porphyrin radical on the UV−vis spectrum of HPC oxidized with PAA. For the $Por-Fe^{IV}-OH$ species, **I***, Fe−O bond lengths of 1.79−1.80 Å are calculated, which are similar to, albeit shorter than, the experimental values observed in HPC (1.80 and 1.85 Å) and to the bond lengths observed in similar structures of MLC, CCP, and BpKatG (Table 1).

A number of explanations are possible for the small discrepancy (0.01 to 0.05 Å) between the Fe−O bond lengths observed in crystal structures and those determined by QM/MM calculations. Experimentally, photoreduction of the Fe−O bond in Cpd I* may have occurred during X-ray exposure.[8,75] It could also be argued that the experimental distances are affected by a sizable error even for a resolution of 1.7 Å. However, the trends observed in Cpd I structures of heme−proteins (Table 1) clearly show that there are two cases, catalases with Fe−O about 1.70 and those with Fe−O about 1.80. Therefore, we do not expect that the error of the experimental structures could be so large to mask these differences. Alternatively, small deviations in the calculated values can be attributed to two main causes. Because of the anharmonicity of the Fe−O vibrational mode, the values obtained from structure optimization (Tables 3 and 4) will shift to slightly longer distances if the dynamics of the Fe−O bond at room temperature are considered. In fact, the Fe−OH distance obtained from first principles MD simulations at room temperature was shown to be 0.02 Å longer than if determined by structure optimization at 0 K.[10] The second source of variability lies in the basis set size, the pseudopotential, and the exchange-correlation functional employed with test calculations using different cutoff values and iron pseudopotentials suggesting variations in the computed Fe=O and Fe−O lengths of ±0.02 and ±0.03, respectively. Taking into consideration these sources of discrepancy, our results support the conclusion that PVC soaked with peroxoacetic acid at pH 5.2 contains predominantly an oxoferryl Fe=O bond, while HPC oxidized at pH 5.6 contains predominantly a hydroxoferryl Fe−OH bond.

Analysis of the spin-density distributions of the oxoferryl models **Ia** and **Ib** in HPC and PVC provides insight into the changes imposed by the presence of different heme types (Figure 1). In HPC, there is spin density on the porphyrin corresponding to one unpaired electron localized on an A_{2u}-like porphyrin orbital. By contrast, the same unpaired electron in PVC is delocalized over the porphyrin, the imidazole of the distal histidine and, to a lesser extent, the axial phenolate. Moreover, the spatial localization of the unpaired spin of PVC changes in response to thermal fluctuations. The different localization of spin density between HPC-**Ia** and PVC-**Ia** can be rationalized in terms of the relative energies of the A_{1u} and A_{2u} porphyrin orbitals which are so similar in energy that small structural variations can easily invert their relative positions, as depicted in Figure 9. In heme d, the formation of the *cis*-hydroxy-γ-spirolactone results in the loss of one double bond in pyrrole ring III, reducing aromatic character in the porphyrin and affecting mainly the A_{1u} orbital which has contributions from the pyrrole β carbon atoms. As a consequence, the energy of the A_{1u} orbital increases relative to the A_{2u} orbital making the "A_{1u}-like" porphyrin orbital the donor of the second oxidation equivalent during compound I formation. Moreover, the imid-

(69) de Visser, S. P.; Shaik, S.; Sharma, P. K.; Kumar, D.; Thiel, W. *J. Am. Chem. Soc.* **2003**, *125*, 15779−15788.
(70) Guallar, V.; Friesner, R. A. *J. Am. Chem. Soc.* **2004**, *126*, 8501−8508.
(71) A. Ivancich. Personal communication.
(72) Jones, P.; Dunford, H. B. *J. Bioinorg. Chem.* **2006**, *99*, 2292−2298.
(73) Mayer, J. M. *Annu. Rev. Phys. Chem.* **2004**, *55*, 363−390.
(74) Kleywegt, G. J.; Jones, T. A. *Acta Crystallogr., Sect. D: Biol. Crystallogr.* **1994**, *50*, 178−185.
(75) Additional QM/MM calculations of the Fe(III)−OH intermediate of HPC show that the Fe−O distance enlarges to 1.81 Å. A similar trend was found in myoglobin (ref 9).

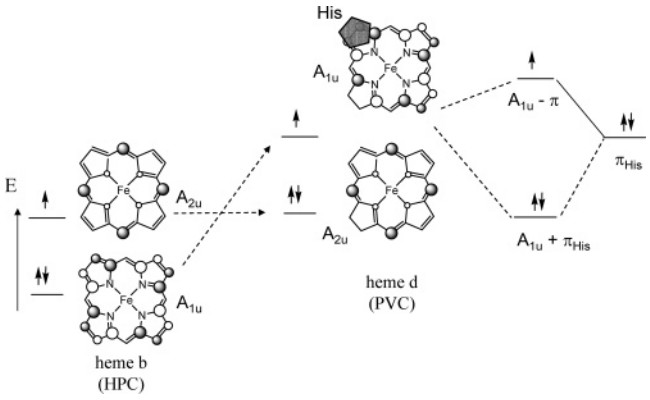

Figure 9. Changes on the relative energy of the A_{1u} and A_{2u} orbitals of the oxoferryl porphyrin species as a result of the heme modification (i.e., upon change from HPC-**Ia** to PVC-**Ia**).

azole of the distal histidine overlaps pyrrole ring IV which carries substantial electron density in the A_{1u} orbital (Figure 6), leading to mixing of the A_{1u} orbital with one π imidazole orbital. As a consequence, the oxidation equivalent from the porphyrin of heme d in PVC is removed from a mixed orbital ($A_{1u}-\pi_{His}$), as reflected in the spin density distribution (Figure 8b). Thus, one of the two electrons removed during oxidation of the heme iron is abstracted from the heme either partially from the porphyrin and the histidine in heme d-containing PVC (Figure 8b) or from only the porphyrin in heme b-containing HPC (Figure 7a). Characterization of compound I in PVC and the closely related HPII of *E. coli* by EPR spectroscopy is planned to test these predictions.

While the radical in compound I is formed initially on the porphyrin, its subsequent migration into the protein was predicted earlier in EPR studies of BLC, CCP, and KatG.[18,22b,24] Reduction of the porphyrin radical allows polarization and lengthening of $Fe^{IV}=O$ to $Fe^{IV}-O^-$ which will rapidly trap a proton to become the hydroxoferryl $Fe^{IV}-OH$. This is formally a proton-coupled electron-transfer mechanism, common in a wide variety of biological systems,[73] and readily explains why quenching of the porphyrin radical and protein radical formation in catalases and peroxidases also involves lengthening and protonation of the oxoferryl unit. Of the main species resulting from heme oxidation (Figure 10), the oxoferryl species **Ia** is formed first and, in the absence of electron transfer from the protein, either **Ia** or its protonated variant **Ib** will accumulate as the classic Cpd I.[72] Species **Ic** is unlikely in light of the expected low pK_a value of the oxoferryl-porphyrin species,[15] and the crystal structure of PVC is consistent with **Ia** and **Ib** being the predominant species present. Electron transfer from the protein to reduce the porphyrin radical and form a protein radical creates **I***, which is isoelectronic in the oxoferryl heme center with classic Cpd II, the intermediate formed by one electron reduction of Cpd I, but with an associated protein radical.

Clearly, current terminology for oxidized catalases and peroxidases is subject to confusion. For example, the structures of MLC, HPC, CCP, and BpKatG with two oxidation equivalents missing from the protein−heme unit should be called Cpd I or Cpd I*, because calling them Cpd II or Cpd II* equates them with the peroxidase reaction intermediate lacking just one oxidation equivalent in the protein−heme unit. UV−vis absorbance spectra, EPR spectra, and X-ray or NMR structure analysis

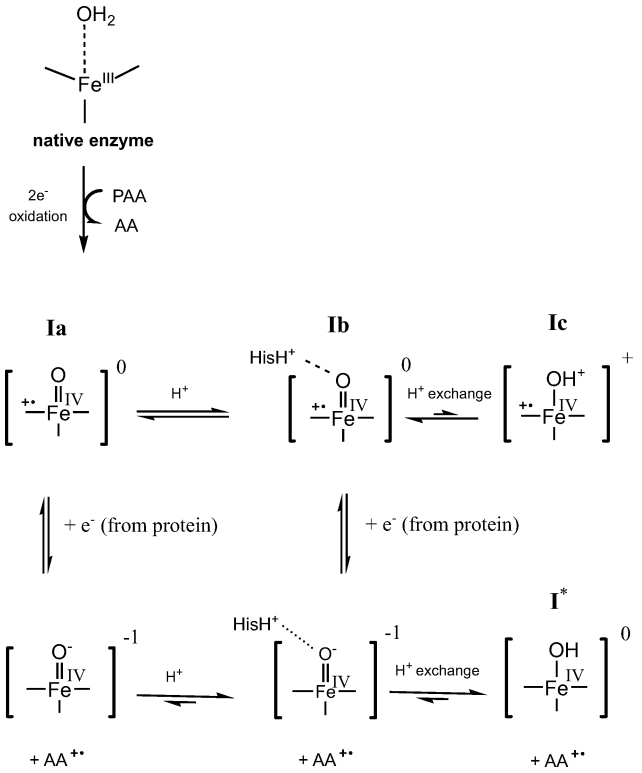

Figure 10. Possible transformations of catalase upon oxidation in the absence of exogenous electron donors. The total charge of the central heme complex is indicated in brackets.

are all essential for the unambiguous identification of reaction intermediates. In addition, terminology must be chosen that accurately reflects the oxidation state of the complete protein−heme unit, not just the heme, which, as the main chromophore, is the focus of UV−vis studies. As an example, Cpd I (or **I*** in this study) of CCP, HPC, MLC, and KatG should be described as a hydroxoferryl $Por-Fe^{IV}-OH$, $AA^{\bullet(+)}$ species, where $AA^{\bullet(+)}$ denotes a protein radical which can be replaced by $Trp^{\bullet+}$ and/or $Tyr^{\bullet}$ in the cases of CCP and KatG where EPR studies have identified the site for the radical formation.[22b,23] In this way the presence and location of the two oxidation equivalents, one on the iron and one in the protein, are clearly delineated. Similarly, Cpd I (or **Ia** and **Ib** in this study) of HRP and PVC should be described as an oxoferryl $Por^{\bullet+}-Fe^{IV}=O$ species, where the second oxidation equivalent is clearly situated on the porphyrin. Reference to the structure of oxidized PMC[31] has been avoided thus far because of the low-resolution 2.5 Å and restraints imposed during refinement which preclude a high confidence in the Fe−O bond length. The reported bond length of 1.76 Å for Fe−O is in between those observed in PVC and HPC but clearly, the EPR spectrum of PMC showed the formation of a stable oxoferryl−porphyrin radical species[17] for the pH range of 5 to 7. In light of crystallization of PMC having been carried out at pH 7.5, the distal histidine is most likely unprotonated and species **Ia** predominates.

Conclusions

The crystal structures of two catalases, HPC and PVC oxidized with peroxoacetic acid to generate an oxoferryl compound I species present different Fe−O bond lengths suggestive of different reaction products. The 1.72 Å iron−oxygen coordination length in PVC is close to what is expected

for a Fe═O double bond and those of 1.80/1.85 Å lengths in HPC are suggestive of a Fe−O single bond. The structure and electronic configuration of the oxidized heme and immediate protein environment have been investigated further by QM/MM density functional theory calculations, considering four different electronic configurations in the heme pocket: $Por^{\bullet+}-Fe^{IV}=O$ (**Ia**), $Por^{\bullet+}-Fe^{IV}=O\cdots HisH^{+}$ (**Ib**), $Por^{\bullet+}-Fe^{IV}-OH^{+}$ (**Ic**), and $Por-Fe^{IV}-OH$ (**I***). The change from heme b (HPC) to heme d (PVC) is mainly reflected in the electronic structure of the oxoferryl form **Ia**. While HPC-**Ia** shows the "standard" porphyrin radical, the same unpaired electron of PVC-**Ia** is shared between the porphyrin and the essential histidine. This can be explained in terms of the change in the relative energies of the porphyrin A_{1u} and A_{2u} orbitals caused by the *cis*-hydroxy-γ-spirolactone modification of the heme in PVC, and measurements are suggested to test these predictions. Comparison of the computational data with the X-ray structures leads to the conclusion that peroxoacetate-treated PVC contains an oxoferryl $Por^{\bullet+}-Fe^{IV}=O$ species with partial protonation of the distal histidine while peroxoacetate-treated HPC contains a hydroxoferryl $Por-Fe^{IV}-OH$ with the second oxidation equivalent delocalized as a protein radical, $AA^{\bullet(+)}$. Therefore, the generalization that the presence of a porphyrin radical is associated with a short Fe−O bond, whereas migration of the porphyrin radical to the protein facilitates protonation and lengthening of the Fe−O bond, is supported both experimentally and by QM/MM density functional theory calculations on the HPC and PVC structures. A simple scheme of the most likely "electronic itinerary" for the primary Cpd I species in catalases is proposed in order to explain these observations.

Acknowledgment. This work was supported by Grants 2005SGR-00036 from the Generalitat de Catalunya and FIS2005-00655 from the Ministerio de Educación y Ciencia (MEC). The computer resources were provided by the Barcelona Supercomputing Center (BSC). X.C. was supported by the Spanish Research Council (CSIC), through the I3P research contract program, and M.A.-P. was supported by a F.I. fellowship from the Generalitat de Catalunya. This work was also supported by Grant OGP9600 from the Natural Sciences and Engineering Research Council of Canada (to P.C.L.) and by the Canadian Research Chair Program (to P.C.L.). We thank Laura Guash (Universitat Rovira i Virgili) for help in analyzing the electronic structure of PVC-**Ia** and Anabella Ivancich for a careful reading of the manuscript.

Supporting Information Available: Figures showing the changes of color of the HPC crystals after PAA soaking, the QM/MM partition used in the calculations, and the fluctuation of the spin density distribution of PVC-**Ia** during the room-temperature molecular dynamics. This material is available free of charge via the Internet at http://pubs.acs.org.

JA063660Y